Journal of Solid State Chemistry 186 (2012) 29–35

Contents lists available at SciVerse ScienceDirect

Journal of Solid State Chemistry

journal homepage: www.elsevier.com/locate/jssc

Biomolecule-assisted synthesis and gas-sensing properties of porous nanosheet-based corundum In_2O_3 microflowers

Wen-Hui Zhang, Wei-De Zhang *

School of Chemistry and Chemical Engineering, South China University of Technology, 381 Wushan Road, Guangzhou 510640, PR China

ARTICLE INFO

Article history:
Received 7 September 2011
Received in revised form
17 November 2011
Accepted 20 November 2011
Available online 1 December 2011

Keywords:
Corundum In_2O_3
Porous
Nanosheets
Microflowers
Gas sensor

ABSTRACT

Porous nanosheet-based corundum In_2O_3 microflowers were fabricated by one-pot hydrothermal treatment of D-fructose and $In(NO_3)_3$ mixture using urea as a precipitating agent followed by calcination. The products were characterized by X-ray diffraction, scanning and transmission electron microscopy. The effects of D-fructose and urea on the fabrication of nanosheet-based corundum In_2O_3 microflowers were investigated and a possible mechanism is proposed to explain the formation of the hierarchical nanostructures. The gas sensor based on the In_2O_3 microflowers exhibits excellent sensing properties for the detection of formaldehyde.

1. Introduction

Indium oxide (In_2O_3), existing in cubic bixbyite and hexagonal corundum, is an important n-type semiconductor with a wide band gap of 3.55–3.75 eV, which holds potential applications in solar cells, optical and electrical devices due to its high optical transparency and electrical conductivity [1]. Although In_2O_3 has been investigated and used for several decades, most In_2O_3 products appear in the form of cubic bixbyite, whereas metastable hexagonal In_2O_3 with corundum structure has rarely been obtained and studied. The corundum In_2O_3 exhibits more stable conductivity than its cubic counterpart [2]. Corundum In_2O_3 was previously obtained under extreme conditions, such as high pressure and high temperature. However, only a few reports have been published concerning with corundum In_2O_3 nanostructures including nanowires, nanotubes, and nanocubes by solvothermal or sol–gel route in organic solvents [2–11]. Sorescu et al. reported that corundum In_2O_3 nanoparticles could be prepared by hydrothermal process under stirring at 200 °C [12]. On the other hand, most nanosheet-based In_2O_3 flower-like structures reported are cubic In_2O_3 [13–15].

Gas sensors based on porous cubic In_2O_3 have also been reported [1,16,17]. Meanwhile, metastable corundum In_2O_3 nanostructures have been prepared for gas sensing. Xu et al. reported that corundum In_2O_3 nanorods are very sensitive to dilute ethanol and H_2S under a heating voltage of 5 V [3], while Fan et al. reported that the gas sensors composed of corundum In_2O_3 microparticles with hierarchical nanostructures exhibited high response and selectivity to 2-chlorophenol at 280 °C with a detection limit of about 5 ppm [6].

Glucose is often used as the template to prepare metal oxide hollow spheres [18–21], while using fructose as the template to prepare metal oxide is rarely studied. In this study, we report the synthesis of corundum In_2O_3 nanosheet-based microflowers inherited from InOOH nanostructures, which were accomplished by D-fructose-assisted hydrothermal process. This green approach involves none of the toxic organic solvents or surfactants and is simple, inexpensive, and productive. The sensor based on nanosheet-based In_2O_3 microflowers shows excellent gas sensing properties to formaldehyde at the relatively low operating temperature of 215 °C.

2. Experimental section

2.1. Preparation and characterization of material

All reagents were of analytical grade without further purification. In a typical preparation procedure, 0.1058 g $In(NO_3)_3 \cdot xH_2O$, 0.432 g D-fructose and 0.064 g urea were added to 16 ml water in a 50 ml Teflon-lined stainless steel autoclave, and stirred for 5 min. The autoclave was then sealed and maintained at 160 °C for 16 h in an oven. After being cooled, the prepared precipitates were collected, washed with distilled water for several time and

* Corresponding author. Fax: +86 20 87114099.
E-mail address: zhangwd@scut.edu.cn (W.-D. Zhang).

0022-4596/$ - see front matter © 2011 Elsevier Inc. All rights reserved.
doi:10.1016/j.jssc.2011.11.031

then dried in air at 60 °C over night. The product was calcined in a furnace at 450 °C for 6 h in air to obtain In_2O_3, and named as Sample 1.

The effect of D-fructose, urea and reaction time on the fabrication of corundum In_2O_3 microflowers was investigated. With other conditions of Sample 1 unchanged, the samples were prepared with different amount of urea of 0, 0.032, 0.192, and 0.384 g, different amount of D-fructose of 0, 0.108, 0.216, and 0.648 g, or different reaction time of 5 and 20 min. The products prepared without urea or D-fructose was named as Samples 2 and 3, respectively.

X-ray diffraction (XRD) analysis was carried out on a Siemens D5005 X-ray diffractometer with Cu$K\alpha$ radiation ($\lambda = 1.5406$ Å). The morphology of the samples was observed by a field emission scanning electron microscope (FESEM) (JEOL JSM-6701F). Transmission electron microscopy (TEM) and high-resolution (HRTEM) measurements were carried out on a FEI Tecnai F20 transmission electron microscope. The Brunauer–Emmett–Teller (BET) surface area was determined by a ST-08A measuring instrument (Beijing Analysis Instruments Technical Company, Beijing, China).

2.2. Fabrication and evaluation of the sensors

Details of gas sensing measurement were reported in our previous paper [22]. The sample was firstly mixed with an organic binder to form a paste. Then, the paste was coated onto an Al_2O_3 tube with two gold leads at each end. After being dried in air, it was sintered at 300 °C for 2 h. Finally, the electrodes were fixed on the circuit for measurement. A heater using Ni–Cr wire was inserted into the Al_2O_3 tube to provide the necessary operation temperature. Resistance of the sensor was measured in air and in sample gases. A chamber was filled with air at 101.3 kPa, and then formaldehyde was injected into the chamber and then evaporated and mixed uniformly with the air by the fans inside. The gas concentration in the chamber was calculated according to the amount of formaldehyde injected and the chamber volume. The response (S) was defined as the ratio (R_a/R_g) of the resistance in air (R_a) and in a sample gas or vapor (R_g). The response/recovery time is defined as the time to reach 90% of the final change in resistance, when the gas is turned on or off, respectively.

3. Results and discussion

3.1. Crystal structure and morphology of Sample 1

The XRD patterns of Sample 1 before and after being calcined at 450 °C for 6 h are shown in Fig. 1(A(a) and (b)), respectively. Before being calcined, all the reflection peaks can be indexed as orthorhombic InOOH (JCPDS 17-0549), and after being calcined, the final product was corundum In_2O_3 (JCPDS 21-0406). Fig. 1(B) and (C) shows the SEM images of Sample 1 before and after being calcined,

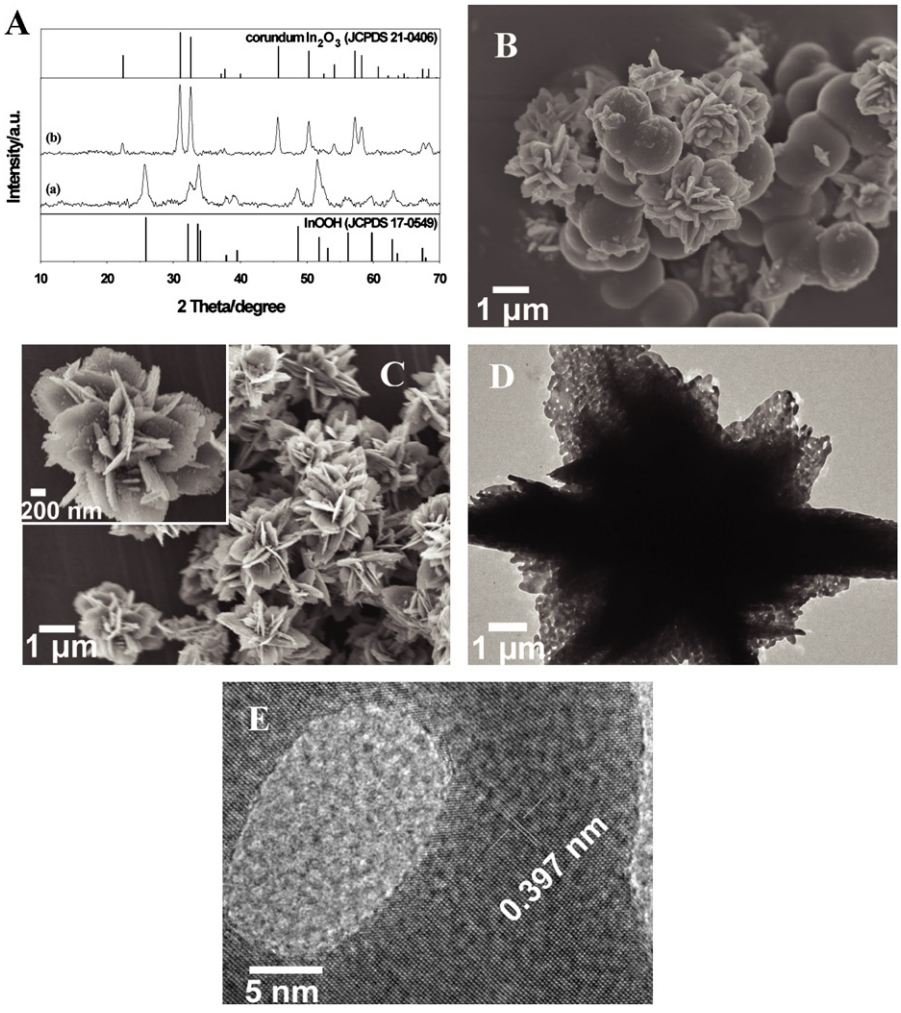

Fig. 1. (A) XRD patterns of Sample 1 (a) before and (b) after being calcined at 450 °C for 6 h, SEM images of Sample 1, (B) before, and (C) after being calcined at 450 °C for 6 h (inset at high magnification), (D) TEM, and (E) HRTEM image of Sample 1 after being calcined.

respectively. Before being calcined, the sample is the mixture of carbon spheres and nanosheet-based microflowers and the thickness of the nanosheets is about 60 nm. After being calcined, carbon spheres which are generated by the decomposition of D-fructose disappeared. The product consists of many microflowers with diameter about 2 μm and these microflowers are built up by many interlaced nanosheets with thickness of about 20 nm and length of several hundred nanometers. Careful observation on the SEM image (Fig. 1(C)) and TEM image (Fig. 1(D)) reveals that the nanosheets are composed of many small nanoparticles. The corresponding HRTEM image (Fig. 1(E)) of a typical microflower exhibits well-defined lattice fringes, indicating their single crystalline nature. The interplanar spacing of 0.397 nm corresponds to the (012) planes of corundum In_2O_3. These results further confirm that the microspheres are corundum structure. It is noted from TEM and HRTEM images that there are many nanopores with different sizes, and their diameter ranges from 10 to 200 nm. Before being calcined, no pores appeared among nanosheets, while after being calcined, the carbon among nanosheets disappeared, leading to the formation of nanopores. The removal of the carbon also results in the decrease of the thickness of the nanosheets.

3.2. Formation of nanosheet-based corundum In_2O_3 microflowers

In this study, a two-step fabrication strategy was employed. Firstly, the InOOH precursor with nanosheet-based microflowers was prepared by a simple hydrothermal route; then, corundum In_2O_3 microflowers were obtained under ambient pressure by the thermal decomposition of the InOOH precursor at 450 °C for 6 h. In order to understand the formation of nanosheet-based corundum In_2O_3 microflowers, we studied the influence of different parameters on the morphology and phase of products systematically. We found that the concentration of D-fructose and urea determine both morphology and crystal phase of In_2O_3 in the final products.

Firstly, the role of D-fructose was investigated. XRD patterns of the samples obtained at different amounts of D-fructose (a) 0, (b) 0.108, (c) 0.216, and (d) 0.648 g before and after being calcined are shown in Fig. 2(A) and (B), respectively. Without D-fructose, the obtained sample was cubic $In(OH)_3$ (JCPDS 73-1810) before being calcined. When D-fructose was increased to 0.108–0.216 g, the prepared samples were mixture of cubic $In(OH)_3$ (JCPDS 73-1810) and orthorhombic InOOH (JCPDS 17-0549), and upon the increase of the amount of D-fructose, the intensity of InOOH increased. Pure InOOH was obtained when D-fructose reached 0.648 g. After being calcined, the sample was cubic In_2O_3 (JCPDS 06-0416) without D-fructose. Upon the increase of the amount of D-fructose, the intensity of corundum In_2O_3 (JCPDS 21-0406) increased and the sample was pure corundum when D-fructose reached 0.648 g. It can be observed that pure InOOH and corundum In_2O_3 can only be obtained with 0.432–0.648 g D-fructose. SEM images of the samples after being calcined at 450 °C for 6 h are shown in Fig. 2(C)–(F). Without D-fructose, cubes were formed. By increasing the amount of D-fructose to 0.108 g, nanosheet-based microflowers appeared, but some nanosheets aggregated together. The morphology was similar to Sample 1 when D-fructose was increased further to 0.216 g. However, more D-fructose (0.648 g) resulted in the decrease of the petals of the microflowers. These experimental results reveal that the amount of D-fructose affects the morphology, and uniform nanosheet-based microflowers can be obtained with 0.216–0.432 g D-fructose. D-fructose molecules have a certain binding affinity to indium ion and can be absorbed onto the nanoparticle surfaces when they start growing, achieving anisotropic crystal growth kinetically. In addition, the rate of primary nucleation is likely to be controlled by the amount of D-fructose. Without D-fructose, $In(OH)_3$ nanocubes are formed. Under low concentration of D-fructose, it is difficult for the primary nanoparticles to assemble into uniform microflowers due to low rate of nucleation. In addition, the formation and aggregation of primary nanoparticles become dominant due to high rate of nucleation with high concentration of D-fructose, and nanosheet-based $In(OH)_3$ microflowers can be obtained. However, when the concentration of D-fructose is very high, microflower structures are destroyed due to the high rate of nucleation.

The amount of urea also plays an important role in determining the morphology of the products. Several experiments with different amounts of urea such as 0, 0.032, 0.192, and 0.384 g with the other conditions unchanged from Sample 1 were conducted. XRD patterns of the samples before and after being calcined are displayed in Fig. 3(A) and (B), respectively. For the sample prepared without urea before being calcined, the peak intensity was very weak, and the phase was unknown. All the peaks of the sample obtained with 0.032 g urea were well indexed to the standard orthorhombic InOOH (JCPDS 17-0549). When urea was increased to 0.192–0.384 g, the prepared samples were the mixture of $In(OH)_3$ and InOOH, and upon the increase of the amount of urea, the intensity of InOOH increased. After being calcined, the peaks of the samples obtained with 0 and 0.032 g urea were well indexed to the standard cubic In_2O_3 and corundum In_2O_3, respectively. With increasing the amount of urea, the intensity of cubic In_2O_3 increased, and cubic In_2O_3 became the main phase when urea reached 0.384 g. It can be concluded that pure corundum In_2O_3 can be achieved with 0.032–0.064 g urea. SEM images of the samples obtained at different amounts of urea are shown in Fig. 3(C) 0 g, (D) 0.032 g, (E) 0.192 g, and (F) 0.384 g. Without urea, the product was mainly hollow microflowers, and some were broken after being calcined. By increasing the amount of urea to 0.032 g, some nanosheet-based microflowers were observed. Further increasing the amount of urea to 0.192 g led to the formation of the mixture of nanosheet-based microflowers and nanorods-based corns with some nanorods growing from the middle (Fig. 3(E)). When more urea (0.384 g) was added, the microflowers disappeared with the corns left only (Fig. 3(F)). The corns are assembled with many nanorods, and these nanorods are attached to each other to form bundles with a length of 730 nm on average. These experimental results reveal that the amount of urea markedly affects the morphologies, and uniform nanosheet-based microflowers In_2O_3 can only be obtained with 0.064 g urea. Upon increasing reaction temperature, the urea molecule begins to hydrolyze to give off NH_3, and the pH value of the solution rises uniformly, which prevents the occurrence of local supersaturation and meanwhile favors the homogeneous nucleation of tiny crystals derived from the complex precursors [14]. As the reaction continues, these crystals aggregate to form nanosheet-based microflowers. When urea is not introduced, there is not enough OH^- in the solution for the full growth of nanosheets, and it is difficult to assemble into nanosheet-based microflowers due to low rate of nucleation, which finally leads to the formation of hollow microspheres. When too much urea is introduced, the formation rate of $In(OH)_3$ is fast, leading to the formation of nanorod-based corns. With appropriate amount of urea, the supply of OH^- via the hydrolysis process is steady and the rate of nucleation is moderate, which results in the final nanosheet-based microflowers.

To study the formation of nanosheet-based corundum In_2O_3 microflowers in detail, time-dependent experiments involved in their growth process at various stages were followed by SEM observation. SEM images of samples hydrothermal treated at 160 °C for 5 min and 20 min are shown in Fig. 4. After 5 min reaction, the product mainly presents single nanosheets and some smaller nanosheets begin to grow from the middle of the single nanosheets. After 20 min, these smaller ones grow bigger, forming nanosheet-based microflowers. For Sampe 1, hydrothermal treatment at 160 °C for 16 h, more uniform nanosheet-based

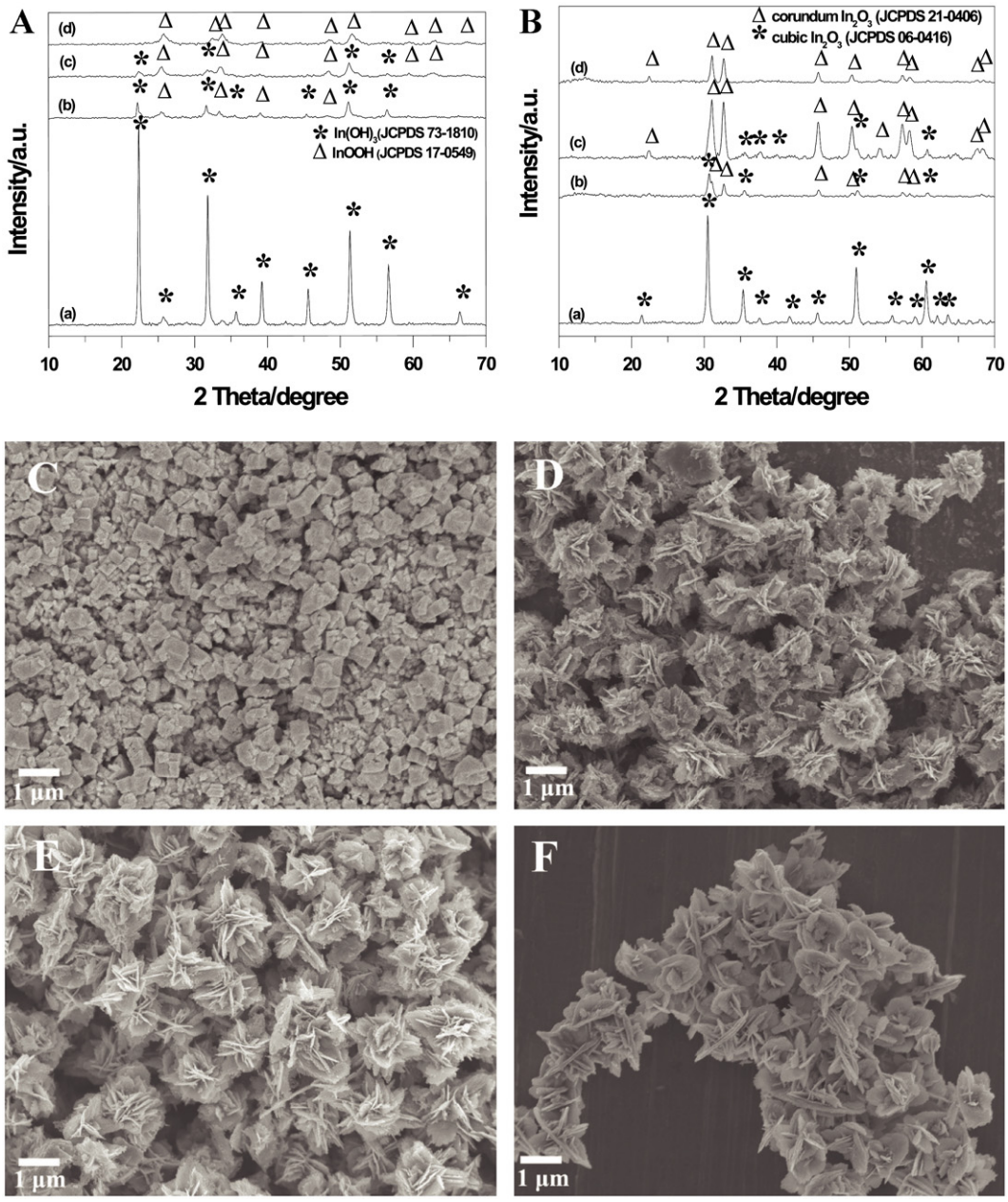

Fig. 2. XRD patterns of the samples (A) before, and (B) after being calcined and prepared with different amounts of D-fructose (a) 0 g, (b) 0.108 g, (c) 0.216 g, and (d) 0.648 g; SEM images of the samples obtained with different amounts of D-fructose (C) 0 g, (D) 0.108 g, (E) 0.216 g, and (F) 0.648 g after being calcined.

microflowers form. It can be seen that nanosheet-based microflowers are assembled from many nanosheets.

3.3. Gas-sensing properties of nanosheet-based In_2O_3 microflowers

The response of gas sensors depends on the operating temperature. In order to determine the optimal operating temperature, the response of the samples to 50 ppm formaldehyde was tested as a function of operating temperature, as indicated in Fig. 5(A). For Sample 1, the response first increases and reaches the maximum ($S=26$) at 190 °C, and then gradually decreases upon the increase of the temperature from 150 to 330 °C. The response of Sample 2 and Sample 3 is lower than that of Sample 1, especially at low operating temperature.

Response and recovery time is also an important parameter of a gas sensor. The response/recovery time of Samples 1–50 ppm formaldehyde at different operating temperature are summarized in Table 1. As is indicated in Table 1, the response time at 150 °C is about 14 s, and it reduces to 10 s at 240–330 °C. The recovery time decreases with the increase of the operating temperature, from 500 s at 150 °C to 5 s at 330 °C. From the above results, one can see that Sample 1 demonstrates rapid response/recovery and relatively higher response ($S=18$) at 215 °C. Therefore, it was selected as the operating temperature in our experiments.

At 215 °C, the typical response/recovery curve of Sample 1 sensor to various concentrations of formaldehyde (5–750 ppm) is displayed in Fig. 5(B). When formaldehyde is introduced, the sensor immediately shows response. In addition, its reversibility and repeatability are also very good. In consecutive tests of the sensor to formaldehyde with various concentrations, the response and recovery is still very good to low concentration of formaldehyde. Fig. 5(C) illustrates the response of Sample 1 to various concentrations of formaldehyde at 215 °C. The sensor exhibits excellent response in the range of 5–750 ppm with the minimum of 5 ppm ($S=6.3$). The response to

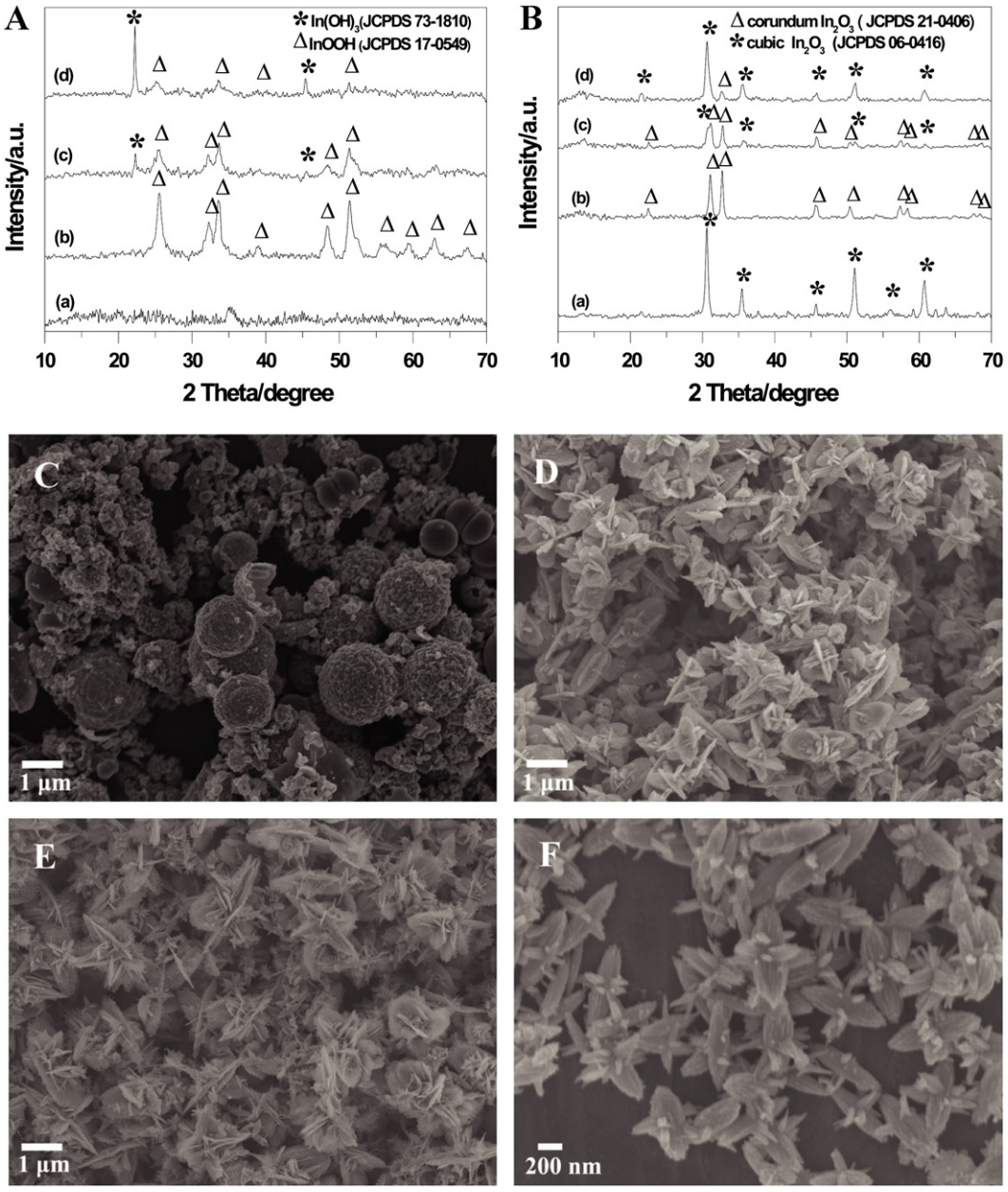

Fig. 3. XRD patterns of the samples (A) before and (B) after being calcined and obtained at different amounts of urea (a) 0 g, (b) 0.032 g, (c) 0.192 g, and (d) 0.384 g; SEM images of the samples obtained at different amounts of urea (C) 0 g, (D) 0.032 g, (E) 0.192 g, and (F) 0.384 g after being calcined.

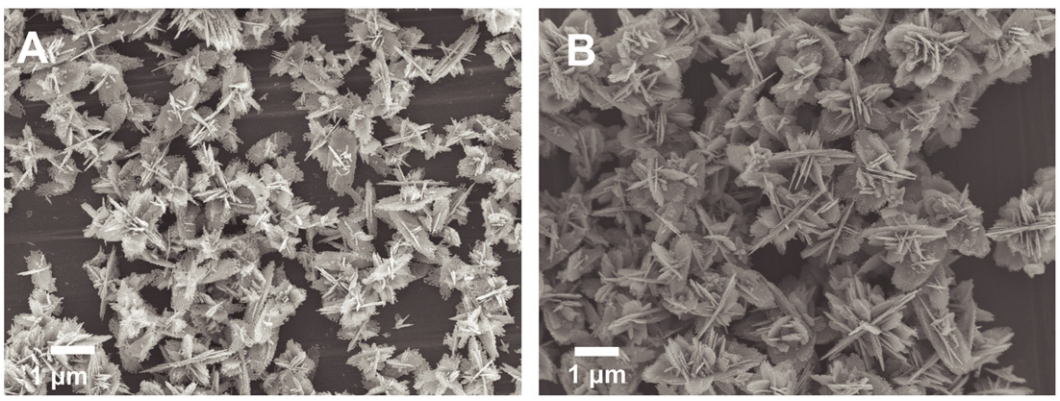

Fig. 4. SEM images of samples hydrothermal treated at 160 °C for (A) 5 min, and (B) 20 min.

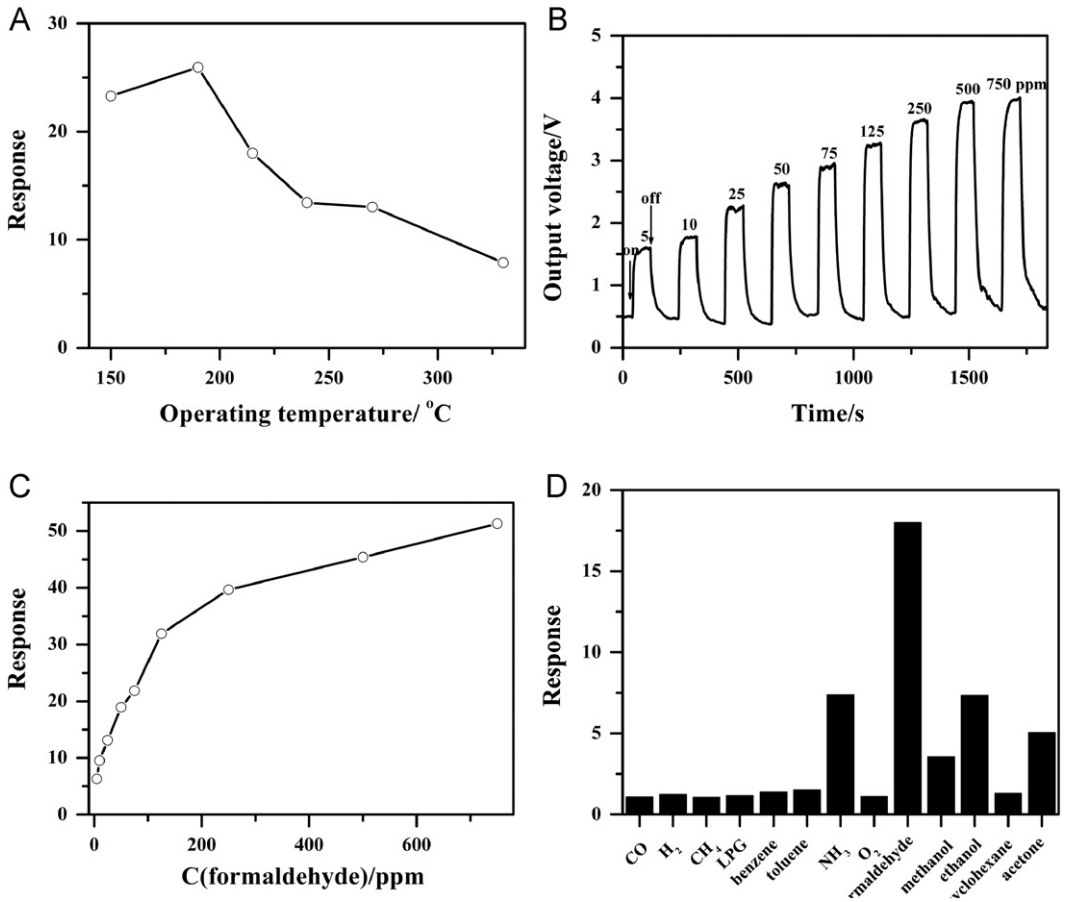

Fig. 5. (A) Responses of the samples to 50 ppm formaldehyde at different operating temperatures. (B) Response/recovery curve and (C) response of Sample 1 sensor to formaldehyde with different concentrations (5–750 ppm) at 215 °C. (D) Response of Sample 1 sensor to various gases or vapors at 215 °C.

Table 1
Response/recovery time of Sample 1 at different operating temperatures.

Operating temperature (°C)	150	190	215	240	270	330
Response time (s)	14	12	11	10	10	10
Recovery time (s)	500	160	30	23	5	5

formaldehyde increases with the increase of its concentration, suggesting that it could meet the application demand. The fast response/recovery characteristics remain when it is used to detect as high concentration of formaldehyde as 750 ppm. The response and recovery time is less than 10 and 60 s, respectively. Thus, it can be concluded that the sensor could detect formaldehyde in the range of 5–750 ppm with prompt response and recovery.

The sensing properties of Sample 1 to other gases or vapors such as CO, H_2, CH_4, ammonia, liquefied petroleum gas (LPG), benzene, toluene, ethanol, methanol, and acetone were also examined. The response to the above gases or vapors of 50 ppm at 215 °C is shown in Fig. 5(D). One can see that this sensor shows the highest response to formaldehyde, while its response to ammonia, ethanol, and acetone is 7.3, 7.3, and 5.1, respectively. The response of the sensor to other gases or vapors such as CO, H_2, NO_2, methane, LPG, etc. is much lower. The above results reveal that this sensor shows high anti-interference ability and could selectively detect formaldehyde.

BET measurements show that the specific surface area of nanosheet-based In_2O_3 microflowers (Sample 1) is 25.3 $m^2 g^{-1}$, while that of hollow spheres (Sample 2) and cubes (Sample 3) is 17.1 and 13.5 $m^2 g^{-1}$, respectively. The unique structure of corundum nanosheet-based In_2O_3 microflowers with larger specific surface area and nanoporous structure provide efficient transport for electrons and offer abundant active sites to the environment. Both are excellent characteristics for potential sensor applications. The sensing mechanism can be elaborated as the following: when nanosheet-based In_2O_3 microflower sensor is exposed to air, oxygen molecules are adsorbed onto the surface of nanosheet-based In_2O_3 microflowers and will form O^{-2}, O^- or O^{2-} ions by capturing an electron from the conductance band of In_2O_3 [23]. Therefore, a space-charge region will be created with In_2O_3 showing a high resistance state in air. When the nanosheet-based In_2O_3 microflowers are exposed to formaldehyde vapor at a moderate temperature, the target molecules are adsorbed onto the surface of the sensors by the formation of hydrogen bonds. Then an oxidation reaction will occur between formaldehyde and the adsorbed oxygen, resulting in the electrons being injected into In_2O_3 and leading to a significant increase in electron concentration. This eventually increases the conductivity of the nanosheet-based In_2O_3 microflowers.

4. Conclusion

In summary, porous nanosheet-based microflowers were prepared by one-pot hydrothermal treatment of D-fructose/$In(NO_3)_3$ mixtures using urea as a precipitating agent at 160 °C for 16 h. By thermal treatment at 450 °C for 6 h, the as-prepared precursors were completely converted into corundum In_2O_3. The amount of D-fructose and urea played almost equally important roles in the morphology and phase of In_2O_3. This simple method is expected to be used for the fabrication of other metal oxides with

controllable phase and morphology. The gas sensor based on the nanosheet-based In_2O_3 microflowers shows swift reaction, high response, and excellent selectivity to 5–750 ppm formaldehyde at 215 °C, which holds great potentials for formaldehyde sensors.

Acknowledgments

Financial support of the work by the Natural Science Foundation of China under Grant 21043005 and Research Fund for the Doctoral Program of Higher Education (RFDP) under Grant 20070561008 is greatly acknowledged.

References

[1] Z. Guo, J.Y. Liu, Y. Jia, X. Chen, F.L. Meng, M.Q. Li, J.H. Liu, Nanotechnology 19 (2008) 345704.
[2] C.H. Lee, M. Kim, T. Kim, A. Kim, J. Paek, J.W. Lee, S.Y. Choi, K. Kim, J.B. Park, K. Lee, J. Am. Chem. Soc. 128 (2006) 9326.
[3] J.Q. Xu, Y.P. Chen, Q.Y. Pan, Q. Xiang, Z.X. Cheng, X.W. Dong, Nanotechnology 18 (2007) 115615.
[4] D.B. Yu, S.H. Yu, S.Y. Zhang, J. Zuo, D.B. Wang, Y.T. Qian, Adv. Funct. Mater. 13 (2003) 497.
[5] M. Epifani, P. Siciliano, A. Gurlo, N. Barsan, U. Weimar, J. Am. Chem. Soc. 126 (2004) 4078.
[6] Y.J. Fan, Z.P. Li, L. Wang, J.H. Zhan, Nanotechnology 20 (2009).
[7] C.L. Chen, D.R. Chen, X.L. Jiao, C.Q. Wang, Chem. Commun. (2006) 4632.
[8] L.Y. Chen, Z.X. Wang, Z.D. Zhang, New J. Chem. 33 (2009) 1109.
[9] H.X. Dong, Z.H. Chen, L.X. Sun, L. Zhou, Y.J. Ling, C.Z. Yu, H.H. Tan, C. Jagadish, X.C. Shen, J. Phys. Chem. C 113 (2009) 10511.
[10] D.B. Yu, D.B. Wang, Y.T. Qian, J. Solid State Chem. 177 (2004) 1230.
[11] Z.B. Zhuang, Q. Peng, J.F. Liu, X. Wang, Y.D. Li, Inorg. Chem. 46 (2007) 5179.
[12] M. Sorescu, L. Diamandescu, D. Tarabasanu-Mihaila, V.S. Teodorescu, J. Mater. Sci. 39 (2004) 675.
[13] C.Q. Wang, D.R. Chen, X.L. Jiao, J. Phys. Chem. C 113 (2009) 7714.
[14] H.Q. Yang, R.G. Zhang, H.X. Dong, J. Yu, W.Y. Yang, D.C. Chen, Cryst. Growth Des. 8 (2008) 3154.
[15] H. Zhu, X.L. Wang, Z.J. Wang, C. Yang, F. Yang, X.R. Yang, J. Phys. Chem. C 112 (2008) 15285.
[16] L. Xu, B.A. Dong, Y. Wang, X. Bai, Q. Liu, H.W. Song, Sens. Actuators B-Chem. 147 (2010) 531.
[17] T. Hyodo, H. Inoue, H. Motomura, K. Matsuo, T. Hashishin, J. Tamaki, Y. Shimizu, M. Egashira, Sens. Actuators B-Chem. 151 (2010) 265.
[18] Y.D. Zhang, G.C. Jiang, K.W. Wong, Z. Zheng, Sens. Lett. 8 (2010) 355.
[19] M.M. Titirici, M. Antonietti, A. Thomas, Chem. Mater. 18 (2006) 3808.
[20] Y.D. Meng, D.R. Chen, X.L. Jiao, Eur. J. Inorg. Chem. (2008) 4019.
[21] J.G. Yu, X.X. Yu, Environ. Sci. Technol. 42 (2008) 4902.
[22] W.H. Zhang, W.D. Zhang, Sens. Actuators B-Chem. 134 (2008) 403.
[23] T. Chen, Q.J. Liu, Z.L. Zhou, Y.D. Wang, Nanotechnology 19 (2008) 095506.